INORGANIC CHEMISTRY FRONTIERS

RESEARCH ARTICLE

View Article Online
View Journal | View Issue

Cite this: *Inorg. Chem. Front.*, 2024, **11**, 1145

Optimized arrangement of non-π-conjugated PO_3NH_3 units leads to enhanced ultraviolet optical nonlinearity in $NaPO_3NH_3$†

Lingli Wu,[a,b,c] Haotian Tian,[b,c] Chensheng Lin, [b] Xin Zhao,[b,c] Huixin Fan,[b] Pengxiang Dong,[b] Shunda Yang,[b] Ning Ye[d] and Min Luo *[a,b]

Received 29th November 2023,
Accepted 2nd January 2024

DOI: 10.1039/d3qi02465b

rsc.li/frontiers-inorganic

The key to achieving nonlinear optical (NLO) crystals with superior optical properties lies in the development of new high-performance functional units and their precise arrangement. In this study, we identify the polar covalent tetrahedron $(PO_3NH_3)^-$, with its remarkable optical properties, as a novel deep-ultraviolet (DUV) NLO-active unit for the first time. To ensure the $(PO_3NH_3)^-$ units are accurately aligned, we selected $NaNH_4PO_3F{\cdot}H_2O$ as a template. Subsequently, we successfully synthesized $NaPO_3NH_3$, wherein the $(PO_3NH_3)^-$ units were arranged in an orderly manner. This excellent ordered arrangement of $(PO_3NH_3)^-$ units enables $NaPO_3NH_3$ to exhibit not only a significant SHG effect (1.2 × KDP), but also the largest birefringence (0.062@546.1 nm) among DUV non-π-conjugated phosphate systems.

Introduction

Deep-ultraviolet (DUV) nonlinear optical (NLO) crystals hold significant potential in extending and regulating laser wavelengths into the DUV region through the frequency-doubling effect. This capability is crucial for applications in semiconductor manufacturing, optical communication, and laser micromachining.[1–4] However, achieving a balance between a short cutoff edge ($\lambda_{cut\text{-}off}$), high second harmonic generation (SHG) efficiency, and moderate birefringence (Δn) remains a challenge for DUV crystals.[5–7] Previous research has indicated that obtaining suitable birefringence for phase matching in DUV crystals is difficult.[8,9] Among the few crystals capable of directly realizing DUV laser output, $KBe_2BO_3F_2$ (KBBF) stands out.[10] Nonetheless, the practical application of KBBF is limited due to its severe layered growth habit and the presence of highly toxic beryllium oxide.

Non-π-conjugated systems have garnered significant interest due to their broader optical transmittance window, making phosphate systems a primary research focus. However, phosphate systems are often hindered by weak SHG and small birefringence, which can be ascribed to the low hyperpolarizability and minimal optical anisotropy resulting from the absence of π orbitals.[11,12] Numerous studies have been conducted to enhance SHG and birefringence in phosphates. One of the most effective approaches involves the use of NLO-active cations, such as Ti^{4+},[13] Bi^{3+},[14] Sn^{2+},[15] and Pb^{2+},[16] among others.[17] Nevertheless, this method invariably induces a red shift of absorption edge, limiting its applicability in the DUV region. To ensure high UV transmission, the selection of cations must be restricted to metal ions with a full shell, including alkali metals, alkaline earth metals, and certain rare earth metal cations.[18–20] Therefore, to maintain the wide band gap of phosphates, an alternative strategy to enhance SHG and birefringence is the modification of $[PO_4]^{3-}$ group.

Along this path, polar polyphosphates, such as P_2O_7 dimer,[21,22] P_3O_{10} trimer,[23,24] and $[PO_3]_\infty$ chain groups,[25,26] have been investigated. However, these crystals exhibit enhancement only in SHG performance. The birefringence of polyphosphates is rarely greater than 0.03@1064 nm, which is attributed to the steric hindrance between groups caused by co-vertex connections, preventing the ordered arrangement of polyphosphate groups. In contrast, isolated tetrahedral groups offer greater flexibility in adjusting their positions to maximize optical anisotropy. Consequently, identifying polar tetrahedral phosphate groups with exceptional properties is

[a]*Fujian Science & Technology Innovation Laboratory for Optoelectronic Information of China, Fuzhou, Fujian, 350108, China. E-mail: lm8901@fjirsm.ac.cn*
[b]*Key Laboratory of Optoelectronic Materials Chemistry and Physics, Fujian Institute of Research on the Structure of Matter, Chinese Academy of Sciences, Fuzhou, Fujian, 350002, China*
[c]*University of the Chinese Academy of Sciences, Beijing, 100049, China*
[d]*Tianjin Key Laboratory of Functional Crystal Materials, Institute of Functional Crystal, Tianjin University of Technology, Tianjin, 300384, China*

†Electronic supplementary information (ESI) available: Crystallographic data and structure date (Tables S1–S5), Dipole moment (Table S6), Comparative table of phosphates (Table S7), and Figures about the measurement results and detail of $NaPO_3NH_3$ (Fig. S1–S7). CCDC 2307797 for $NaPO_3NH_3$. See DOI: https://doi.org/10.1039/d3qi02465b

crucial. In light of this, Pan and Chen (2018) groups proposed introducing highly electronegative fluorine (F) into $[PO_4]^{3-}$ groups to obtain polar $(PO_3F)^{2-}$ with excellent DUV optical properties. Subsequent studies discovered crystals such as $(NH_4)_2PO_3F$ [27] and $[C(NH_2)_3]_2PO_3F$;[28] however, the arrangement of polar tetrahedral groups in these crystals did not favor maximizing enhanced birefringence. In 2019, Chen's group successfully synthesized and grew $NaNH_4PO_3F{\cdot}H_2O$,[29] which binds fluorophosphate together through hydrogen bonds from NH_4^+, achieving near-directional arrangement of non-π-conjugated DUV functional units of polar phosphate units for the first time. Ultimately, $NaNH_4PO_3F{\cdot}H_2O$ exhibited a large SHG and an extremely prominent birefringence of >0.053@589.3 nm while maintaining deep-ultraviolet transmittance. Given that $NaNH_4PO_3F{\cdot}H_2O$ has been demonstrated to be an outstanding DUV NLO crystal, it potentially serves as a novel parent compound to guide the synthesis and screening of new materials.

In the investigation of the sulfonate system, our research group has discovered that polar tetrahedra, obtained by employing substituents such as amino and methyl groups, exhibit exceptional DUV optical properties.[30,31] Consequently, we have identified a series of DUV non-π-conjugated NLO crystals with outstanding characteristics, including $M(SO_3NH_2)_2$ (M = Ba, Sr),[32] sulfamide,[33] and $KNO_3SO_3NH_3$.[34] Compared to $(SO_4)^{2-}$, $(NH_2SO_3)^-$ and $SO_2(NH_2)_2$ demonstrate superior performance in three key aspects: polarizability anisotropy, hyperpolarizability, and the highest occupied molecular orbital (HOMO)–lowest unoccupied molecular orbital (LUMO) gap. Moreover, the incorporation of hydrogen-containing anionic groups facilitates the regulation of their arrangement. For instance, sulfamide employs the hydrogen bond of $SO_2(NH_2)_2$ to align itself unidirectionally within a layer. Since the geometric structure and optical properties of PO_4 closely resemble those of SO_4, we anticipate that modifying the phosphate group with amino or methyl groups could yield a novel polar tetrahedron containing hydrogen bonds and possessing exceptional optical properties.

In this study, we employed $NaNH_4PO_3F{\cdot}H_2O$ as a template. By replacing F^- with an NH_3 group, we formed the new polar tetrahedron $(PO_3NH_3)^-$, with the expectation that it would display excellent DUV optical properties and achieve a consistent arrangement through its inherent hydrogen bond. Furthermore, our calculations revealed that the polar $(PO_3NH_3)^-$ unit exhibits improved performance in the aforementioned three key aspects compared to $(PO_4)^{3-}$. Encouraged by these computational findings, we successfully synthesized an amino-phosphate DUV NLO material, $NaPO_3NH_3$ (NPNH). Notably, the polar $[PO_3NH_3]^-$ groups in NPNH achieved optimal alignment, which significantly enhanced the (010) in-plane anisotropy and resulted in the largest Δn (0.062) reported to date among DUV non-π-conjugated phosphate systems. Physical measurements demonstrated that NPNH exhibits a substantial second-harmonic generation (SHG) effect (1.2 × KH_2PO_4 (KDP)) and short cutoff edges (<190 nm).

Experimental section

Reagents

Diphenyl Phosphoramidate ($C_{12}H_{12}NO_3P$, 97%, Adamas), NaOH (≧98%, Titan), Gelatin (Aladdin), Acetic acid glacial (≧99.5%, Titan).

Synthesis

Polycrystalline samples of $NaPO_3NH_3$ were synthesized according to the method described by E. Hobbs, D. E. C. Corbridge, and B. Raistrick.[35] A mixture of Diphenyl Phosphoramidate (8 mmol, 1.994 g), NaOH (32 mmol, 1.280 g), and H_2O (10 ml) was heated until the Diphenyl Phosphoramidate was completely hydrolyzed. Then acetic acid glacial was slowly dripped into the solution and the insoluble monosodium salt ($NaPO_3NH_3$) was produced according to the following scheme:

$$(PhO)_2PONH_2 \xrightarrow{NaOH} (NaO)_2PONH_2 \xrightarrow[HO]{HAc\ NaO} > PONH_2(NaPO_3NH_3)$$

However, the insoluble nature of $NaPO_3NH_3$ prevented the growth of the required crystals from a simple solution. Thus, we adopted the method of crystallizing within the gelatin gels in a U-tube to obtain large crystals for subsequent measurements. For this purpose, the gelatin (1 g) was soaked in 15 ml H_2O for 5 minutes and then heated until the gelatin was dissolved. Next, the gelatin solution was poured into a U-tube for 3 hours to solidify. Finally, the solution of $(NaO)_2PONH_2$ (10 ml, previously prepared) and acetic acid glacial (10 ml) were filled into the respective arms of the U-tube. After one week, a small number of transparent colorless polycrystalline $NaPO_3NH_3$ crystals were obtained. These crystals were stable in the air and hardly water-soluble.

Single-crystal X-ray diffraction

For single-crystal X-ray diffraction measurement, a premium $NaPO_3NH_3$ signal crystal was chosen. The graphite-monochromatic Cu-Kα radiation (λ = 1.54184 Å) was used to acquire the diffraction data by using a Rigaku Mercury CCD diffractometer at room temperature. The data was integrated by the Crystal Clear program. The intensities were corrected by Lorentz polarization, air absorption, and absorption attributable to the variation in the path length through the detector faceplate. The crystal structure of $NaPO_3NH_3$ was solved through the directed methods and then confirmed by full-matrix least-squares fitting on F^2 using SHELXL on the Olex2 package.[36,37] The PLATON program was used to check for the structure, and no higher symmetry was found. Crystallographic data and structure refinements of $NaPO_3NH_3$ were given in Table S1.† Atomic coordinates, equivalent isotropic displacement parameters, selected bond lengths and angles, and anisotropic displacement parameters for $NaPO_3NH_3$ were shown in Tables S2–S4.†

Power X-ray diffraction

The power X-ray diffraction (XRD) patterns were collected on the Miniflex-600 powder X-ray diffractometer (Cu Kα radiation

with λ = 1.540598 Å) from 10° to 80° at room temperature with a scanning speed of 5° min^{-1}. The experimental powder XRD patterns and the simulated patterns of the single crystal are coincident.

Energy-dispersive X-ray spectroscopy analysis

Energy dispersive X-ray spectroscopy (EDS) was tested on the FESEM, SU-8010 scanning electron microscope (SEM) with an X-ray spectroscope. A clean $NaPO_3NH_3$ crystal was mounted on an aluminum sample stage with carbon conductive tape.

Thermal analysis

The data thermogravimetric analysis (TG) and differential thermal analysis (DTA) were carried out on the Netzsch STA449C simultaneous analyzer. $NaPO_3NH_3$ power was packed in an Al_2O_3 crucible and heated from room temperature to 900 °C at a rate of 10 °C min^{-1}.

UV-Vis diffuse reflectance spectroscopy

The UV-Vis diffuse reflection spectrum was measured on PerkinElmer Lamda-950 UV-Vis spectrophotometer scanning with the scope of 190–800 nm to determine the cutoff edge of the $NaPO_3NH_3$ crystal. $BaSO_4$ is used as the standard of 100% reflectance.

Birefringence measurement

The birefringence measurement was performed on the polarizing microscope (ZEISS Axio Scope. A1) equipped with a Berek compensator. The light source is 546.1 nm. The formula for calculating is expressed as follows: $\Delta n = \Delta R/T$, while ΔR means the optical path difference, Δn signifies the birefringence, and T represents the thickness of the crystal.

Second harmonic generation measurements

The test of polycrystalline powder Second Harmonic Generation (SHG) was executed on a Q-switched Nd: YAG solid-state laser with laser radiation wavelengths of 1064 nm. The sample was divided into 24–45, 45–62, 62–75, 75–109, 109–150, and 150–212 μm, respectively. KH_2PO_4 (KDP) is used as the standard reference. The samples were pressed between two round glass plates, each sealed with 8 mm diameter and 1 mm thick rubber rings. Then the samples were placed in the antiglare box and irradiated with the pulsed laser from an OPO laser. The signals are detected with a photomultiplier tube connected to a RIGOL DS1052E 50 MHz oscilloscope. The ratio of the SHG intensity outputs for the samples and KDP was calculated.

Theoretical calculations

The molecular orbitals and polarizability calculations were carried out using density functional theory (DFT)[38] and couple cluster with singles and doubles substitutions (CCSD) implemented in the Gaussian09 package 41. HOMO–LUMO Gap (E_g) of anionic groups were calculated through CCSD/Aug-cc-PVDZ, and the polarizability anisotropy (δ) and hyperpolarizability tensor were calculated through wB97/Aug-cc-PVDZ.

Band structure and density of states (DOS) were determined using DFT calculations provided by the CASTEP code in the Material Studio Package. The exchange interaction[38] was treated by the generalized gradient approximation (GGA) of Perdew–Burke–Ernzerhof (PBE).[39] The energy cutoff for the plane wave was chosen as 750 eV, and the Monkhorst–Pack k-point sampling of 2 × 2 × 2 in the Brillouin zone of the unit cell was selected for calculation. The valence electrons are Na $2s^2\ 2p^6\ 3s^1$, P $3s^2\ 3p^3$, O $2s^2\ 2p^4$, N $2s^2\ 2p^3$, and H 1s. The real part of the dielectric function was obtained by the Kramers–Kronig transform, and then the refractive index was determined. The SHG coefficients were obtained by the formula originally proposed by Sipe *et al.*[40] and developed by Cheng *et al.*[41] The SHG density of d_{33} is calculated out by the band-resolved method.[42]

Results and discussion

In order to investigate the potential structure-directing optical properties of amino-phosphate, we performed calculations and constructed molecular orbital diagrams for phosphate family groups. As shown in Fig. 1 HOMO, the nonbonding O 2p orbitals occupied the HOMO in three groups, while the F atom and NH_3 group were not involved. This indicates that the electrons within the group are not evenly distributed, suggesting that the polarizability anisotropy values of $(PO_3F)^{2-}$ and $(PO_3NH_3)^-$ are not lower than those of $(PO_4)^{3-}$. From HOMO to LUMO, the electron distribution in $(PO_3NH_3)^-$ shifts from O to NH_3. This extensive electron redistribution correlates with a large electric field, which may enhance the SHG effect. Additionally, we calculated three parameters for $(PO_4)^{3-}$, $(PO_3F)^{2-}$ and $(PO_3NH_3)^-$ as references (Table 1). The computed HOMO–LUMO gap of $(PO_3NH_3)^-$ is comparable to that of $(PO_4)^{3-}$, suggesting that amino-phosphate could maintain the

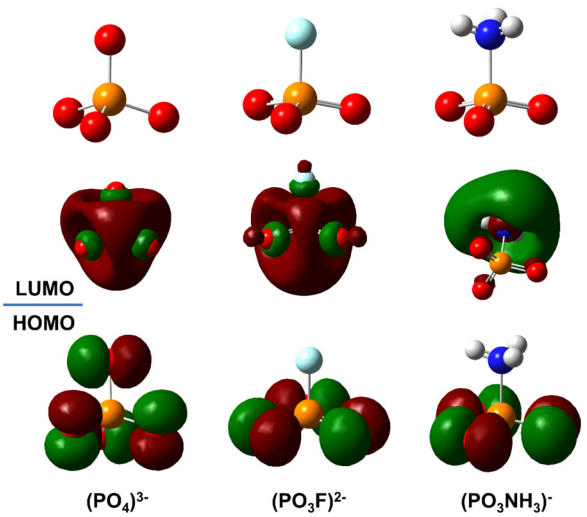

Fig. 1 Molecular orbitals of the $(PO_4)^{3-}$, $(PO_3F)^{2-}$, and $(PO_3NH_3)^-$ anionic groups. The HOMO and LUMO are shown in the middle and lower panels, respectively.

Table 1 Calculated properties of the optimized $(PO_4)^{3-}$, $(PO_3F)^{2-}$ and $(PO_3NH_3)^-$ groups

Units	δ	$\|\beta\|$	E_g (eV)
$(PO_4)^{3-}$	0	0	7.24
$(PO_3F)^{2-}$	6.03	60.8	9.52
$(PO_3NH_3)^-$	2.16	194	7.82

Polarizability anisotropy (δ), hyperpolarizability tensor (β), and HOMO–LUMO gap (E_g).

advantage of broad UV transmittance characteristic of phosphate. Concurrently, $(PO_3NH_3)^-$ exhibits superior hyperpolarizability, which can be rationalized by the values of the "flexible" chemical bonds within the NLO-active group.[43] The flexibility index of P–N in $(PO_3NH_3)^-$ (F = 0.14) is greater than that of P–F in $(PO_3F)^{2-}$ (F = 0.09), indicating that the more flexible P–N bonds are beneficial for further enhancing the SHG response. In conclusion, based on anionic group theory, the slightly larger polarizability anisotropy and superior hyperpolarizability could result in exceptional NLO properties.

$NaPO_3NH_3$ (NPNH) powder samples were synthesized using the two-step method reported by E. Hobbs *et al.*[35] To obtain large crystals for subsequent measurements, we employed a U-tube gelatin gel crystallization technique. The experimental powder X-ray diffraction (PXRD) pattern in Fig. S1† is consistent with the calculated values, confirming phase purity. Energy-dispersive X-ray spectroscopy (EDS) analysis reveals that the crystal contains Na, P, O, and N elements (Fig. S2†). Thermogravimetric (TG) and differential thermal analysis (DTA) curves for NPNH are presented in Fig. S3,† indicating stability up to 260 °C, which is higher than the thermal stability of $NaNH_4PO_3F{\cdot}H_2O$ (under 100 °C),[29] $KNO_3SO_3NH_3$ (~150 °C),[34] and $KLi(HC_3N_3O_3){\cdot}2H_2O$ (125 °C).[44] NPNH is insoluble in water and alcohol and remains stable in air at room temperature for at least three months.

NPNH crystallizes in the hexagonal asymmetric space group $P6_3$ (No. 173) with lattice parameters a = 5.7805(1) Å, c = 6.0265 (1) Å, which aligns with the findings of E. Hobbs *et al.* The structure of NPNH is characterized by a single anionic structural motif, $(PO_3NH_3)^-$. As illustrated in Fig. 2d, each phosphorus atom is tetrahedrally coordinated by three oxygen atoms and an NH_3 group, forming a $(PO_3NH_3)^-$ tetrahedron. The P–O distances are approximately 1.509 Å, and the P–N bond length is 1.779 Å. Intriguingly, the $(PO_3NH_3)^-$ groups are interconnected *via* hydrogen bonds, facilitating the formation of a three-dimensional (3D) structure in NPNH. Sodium cations are embedded within this network, ensuring overall charge neutrality (Fig. 2b). This bonding pattern is reminiscent of the interactions observed between $(PO_3F)^{2-}$ groups in $NaNH_4PO_3F{\cdot}H_2O$. When contrasted with $NaNH_4PO_3F{\cdot}H_2O$, NPNH exhibits a more neatly arrangement of anionic groups (Fig. 2e and f). In $NaNH_4PO_3F{\cdot}H_2O$, the $(PO_3F)^{2-}$ tetrahedra within each layer are anchored by water molecules and NH_4^+ groups, forming a robust hydrogen-bonded network that aligns nearly parallel to the c-axis. In contrast, in NPNH, the $(PO_3F)^{2-}$ and NH_4^+ groups are combined into a single $(PO_3NH_3)^-$ group (Fig. 2c and d), and $(PO_3NH_3)^-$ units are able

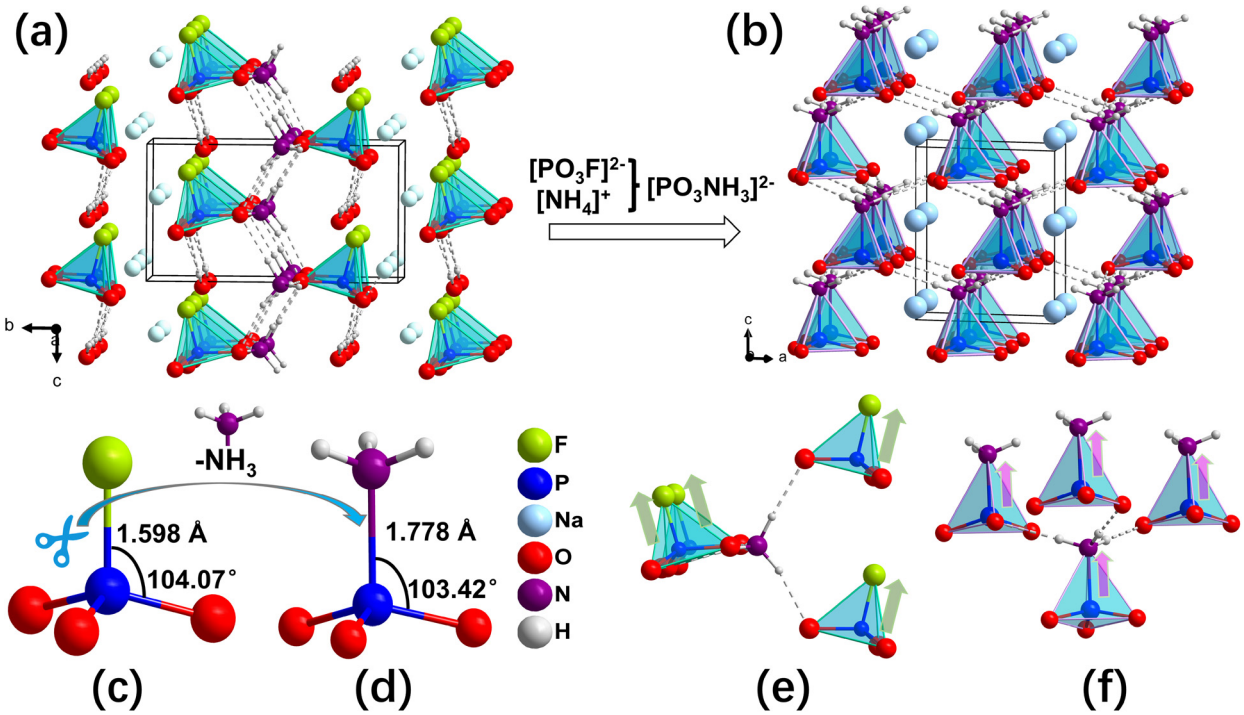

Fig. 2 (a) the structure of $NaNH_4PO_3F{\cdot}H_2O$; (b) the structure of $NaPO_3NH_3$; (c and d) transformation from $[PO_3F]^{2-}$ to $[PO_3NH_3]^-$; (e and f) the arrangement of anionic groups in $NaNH_4PO_3F{\cdot}H_2O$ and $NaPO_3NH_3$, respectively.

to achieve complete alignment along the *c*-axis due to their inherent hydrogen bonds (Fig. 2a and b). Consequently, this uniform alignment of polar P–N bonds results in the superposition of dipoles along the *c*-axis, maximizing macroscopic polarization. This leads to a significant enhancement of the (010) in-plane anisotropy, enabling NPNH to exhibit birefringence along the *c*-axis. Furthermore, the hydrogen bonds between anions and Na–O ionic bonds give rise to a 3D structure without any layering tendency (Fig. S4†). The lack of crystal water in NPNH potentially enhances its thermal stability.

The Ultraviolet–Visible (UV-Vis) diffuse reflectance spectra of NPNH are presented in Fig. 3a, illustrating an absorption edge below 190 nm, which corresponds to a band gap exceeding 6.5 eV. The electronic and optical properties of NPNH were computed using the first-principles method, indicating a band gap of 5.320 eV (Fig. S5†). The discrepancy between the experimental and computed band gaps can be attributed to the discontinuity of the exchange–correlation energy function.

The SHG response of NPNH was evaluated under fundamental wave laser radiation (λ = 1064 nm), utilizing polycrystalline KDP as a reference. As depicted in Fig. 3b, the SHG response of NPNH is approximately 1.2 times that of KDP within the particle size range of 150–212 μm, exhibiting phase-matchable behavior in accordance with the rule proposed by Kurtz and Perry.[45] Given that the space group is $P6_3$, two independent SHG tensor components (d_{31}, d_{33}) must be considered. Through the application of the "velocity-gauge" formula developed by Sipe *et al.*,[40,46] the largest tensor component d_{33} of NPNH is 0.583 pm V^{-1} at a wavelength of 1064 nm (1.165 eV), while the largest tensor component d_{14} of KDP is 0.381 pm V^{-1} at the same wavelength (Fig. S6†). Accordingly, the calculated SHG intensity is approximately 1.5 times that of KDP, aligning closely with the experimental value. Furthermore, the SHG-weighted electron density of d_{33} was investigated to discern the origin of the SHG responses (refer to Fig. 3c and d). The occupied and unoccupied states suggest that the primary SHG effect stems from the $(PO_3NH_3)^-$ units, which is consistent with the anionic group theory.[47]

The birefringence measurement was conducted using a ZEISS Axio Scope. A1 polarizing microscope, equipped with a Berek compensator. The resultant values for ΔR and T were 1219.7 nm and 19.64 μm, respectively, as shown in Fig. S7† and Fig. 4a. The calculated birefringence at 546.1 nm, derived using the formula $\Delta n = \Delta R/T$,[48] was 0.062, closely aligning with the theoretical value of 0.063, following the trend of $n_a = n_b > n_c$ (Fig. 4b). It is concluded that NPNH exhibits the highest birefringence among DUV phosphates, surpassing that of $NaNH_4PO_3F{\cdot}H_2O$ (0.053@589.3 nm), as illustrated in Fig. 4e and Table S7.† This significant birefringence can be primarily attributed to two reasons. First, the $(PO_3NH_3)^-$ unit displays a greater polarizability anisotropy, which contributes to enhanced birefringence. Second, these units possess an

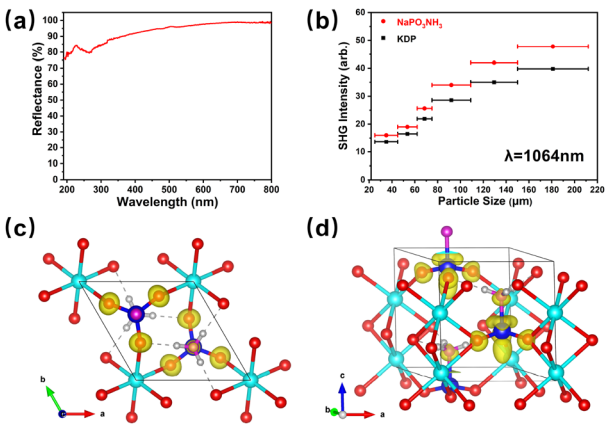

Fig. 3 (a) The UV/Vis diffuse-reflectance spectroscopy of $NaPO_3NH_3$; (b) power SHG measurement at 532 nm; (c and d) the SHG density of d_{33} in occupied state and unoccupied state.

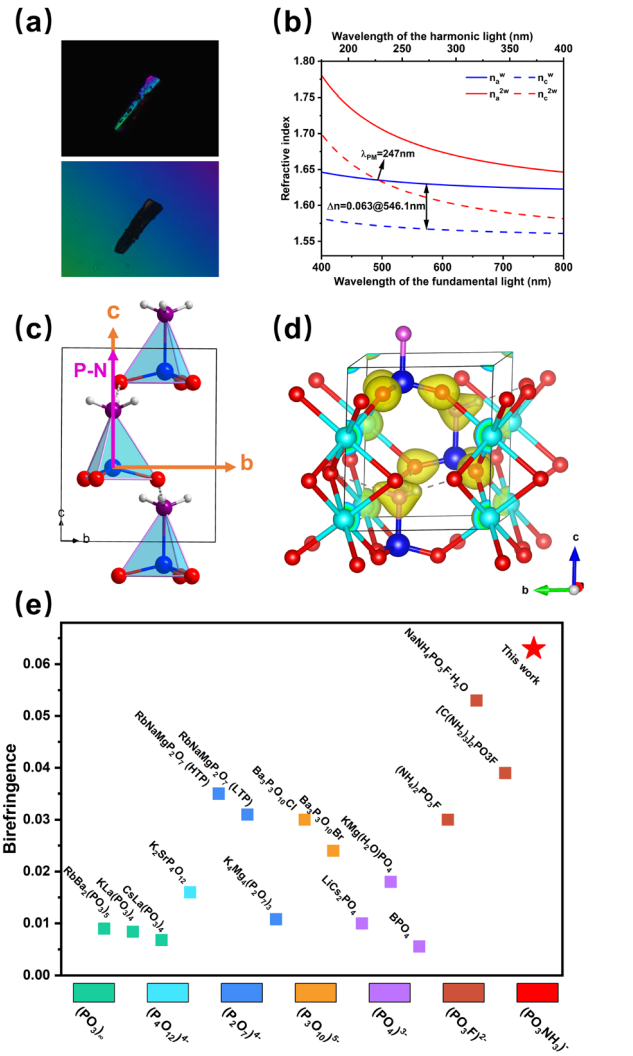

Fig. 4 (a) Photograph of $NaPO_3NH_3$ in the size of 19.64 μm; (b) calculated the refractive index of $NaPO_3NH_3$; (c) the angular correlation between the P–N bond and the crystallophysical axis *c* is 0°; (d) the calculated electron density map of NPNH; (e) the birefringence of phosphates whose $\lambda_{cut\text{-}off}$ below 200 nm.

optimal arrangement, superior to that of $NaNH_4PO_3F{\cdot}H_2O$, as the angle between the P–N bond and the crystallophysical axis *c* is eliminated (Fig. 4c). The computed dipole moment, as shown in Table S6,† vividly reflects this optimized arrangement. The net dipole moment of $(PO_3NH_3)^-$ units is calculated to be 10.02 D in the polar *c* direction, with 0 D on the *a* and *b* directions, indicating that the polarization direction of all $(PO_3NH_3)^-$ units is along the *c*-axis. This optimal arrangement potentially compensates for the diminished birefringence effect caused by the reduced anisotropy of the $(PO_3NH_3)^-$ unit compared to $(PO_3F)^{2-}$. As shown in Fig. 4d, the uniform arrangement of polar chemical bonds considerably reduces the electron density in the *c*-axis direction, resulting in a significant decrease in electron density in the *c* direction compared to the *a* and *b* directions. Consequently, the refractive index in the *c* direction is substantially lower than that in the *a* and *b* directions, leading to high birefringence.[49] This is further corroborated by the calculated refractive index dispersion curve.

Conclusions

We report the successful synthesis and growth of a novel NLO crystal, $NaPO_3NH_3$, utilizing the newly developed polar NLO-active $(PO_3NH_3)^-$ unit. Structural analysis reveals that these polar $(PO_3NH_3)^-$ units achieve complete alignment along the *c*-axis, resulting in a uniform arrangement of polar P–N bonds. This unique alignment facilitates the superposition of dipoles along the *c*-axis, thereby maximizing macroscopic polarization. The resultant effect is an enhanced SHG response and a significantly amplified (010) in-plane anisotropy. Furthermore, $NaPO_3NH_3$ demonstrates a DUV absorption edge, indicating its potential as a promising DUV NLO crystal. This study not only introduces a novel NLO phosphate anion group but also proposes a new strategy for obtaining NLO crystals with large birefringence.

Author contributions

Prof. Min Luo provided research ideas, supervised the entire research, and revised the manuscript. Lingli Wu wrote the initial draft and completed the entire experiment and measurement work. Haotian Tian assisted in the experiments and measurements. Dr Chengshen Lin and Xin Zhao were responsible for theoretical calculations. Dr Huixin Fan, Pengxiang Dong, Dr Shunda Yang, and Prof. Ning Ye offered help with data and experiment analysis. All authors participated in the discussion.

Conflicts of interest

The authors declare no competing financial interests.

Acknowledgements

This work was supported by the National Natural Science Foundation of China (Grant No. 22222510, 21975255, 21921001, and 52302008), the Natural Science Foundation of Fujian Province (2023J02026), the Foundation of Fujian Science & Technology Innovation Laboratory (2021ZR202), and the Self-deployment Project Research Program of Haixi Institutes, Chinese Academy of Sciences (CXZX-2022-JQ01).

References

1 N. Savage, Ultraviolet lasers, *Nat. Photonics*, 2007, **1**, 83–85.
2 D. Cyranoski, China's crystal cache: a Chinese laboratory is the only source of a valuable crystal. David Cyranoski investigates why it won't share its supplies, *Nature*, 2009, **457**, 953–955.
3 F. Xu, G. Zhang, M. Luo, G. Peng, Y. Chen, T. Yan and N. Ye, A powder method for the high-efficacy evaluation of electro-optic crystals, *Natl. Sci. Rev.*, 2021, **8**, nwaa104.
4 K. C. Chen, C. S. Lin, J. D. Chen, G. S. Yang, H. T. Tian, M. Luo, T. Yan, Z. Hu, J. Wang, Y. Wu, N. Ye and G. Peng, Intense *d-p* Hybridization in Nb_3O_{15} Tripolymer Induced the Largest Second Harmonic Generation Response and Birefringence in Germanates, *Angew. Chem.*, 2023, **135**, e202217039.
5 P. S. Halasyamani and J. M. Rondinelli, The must-have and nice-to-have experimental and computational requirements for functional frequency doubling deep-UV crystals, *Nat. Commun.*, 2018, **9**, 2972.
6 L. Kang, S. Y. Luo, G. Peng, N. Ye, Y. C. Wu, C. T. Chen and Z. S. Lin, First-Principles Design of a Deep-Ultraviolet Nonlinear-Optical Crystal from $KBe_2BO_3F_2$ to $NH_4Be_2BO_3F_2$, *Inorg. Chem.*, 2015, **54**, 10533–10535.
7 L. Xiong, J. Chen, J. Lu, C. Y. Pan and L. M. Wu, Monofluorophosphates: A New Source of Deep-Ultraviolet Nonlinear Optical Materials, *Chem. Mater.*, 2018, **30**, 7823–7830.
8 C. C. Jin, F. M. Li, X. Q. Li, J. J. Lu, Z. H. Yang, S. L. Pan and M. Mutailipu, Difluoro (oxalato) borates as Short-Wavelength Optical Crystals with Bifunctional $[BF_2C_2O_4]$ Units, *Chem. Mater.*, 2022, **34**, 7516.
9 H. T. Qiu, F. M. Li, Z. H. Yang, S. L. Pan and M. Mutailipu, Breaking the Inherent Interarrangement of $[B_3O_6]$ Clusters for Nonlinear Optics with Orbital Hybridization Enhancement, *J. Am. Chem. Soc.*, 2023, **145**, 24401–24407.
10 C. T. Chen, G. L. Wang, X. Y. Wang and Z. Y. Xu, Deep-UV nonlinear optical crystal $KBe_2BO_3F_2$—discovery, growth, optical properties and applications, *Appl. Phys. B: Lasers Opt.*, 2009, **97**, 9–25.
11 W. Q. Huang, S. G. Zhao and J. H. Luo, Recent Development of Non-π-Conjugated Deep Ultraviolet Nonlinear Optical Materials, *Chem. Mater.*, 2022, **34**, 5–28.
12 Y. Q. Li, J. H. Luo and S. G. Zhao, Local Polarity-Induced Assembly of Second-Order Nonlinear Optical Materials, *Acc. Chem. Res.*, 2022, **55**, 3460–3469.

13 P. S. Halasyamani, Asymmetric Cation Coordination in Oxide Materials: Influence of Lone-Pair Cations on the Intra-octahedral Distortion in d0 Transition Metals, *Chem. Mater.*, 2004, **16**, 3586–3592.
14 D. Chen, S. Hao, L. Fan, Y. Guo, J. Yao, C. Wolverton, M. G. Kanatzidis, J. Zhao and Q. Liu, Broad Photoluminescence and Second-Harmonic Generation in the Noncentrosymmetric Organic–Inorganic Hybrid Halide $(C_6H_5(CH_2)_4NH_3)_4MX_7{\cdot}H_2O$ (M = Bi, In, X = Br or I), *Chem. Mater.*, 2021, **33**, 8106–8111.
15 J. Y. Guo, A. Tudi, S. J. Han, Z. H. Yang and S. L. Pan, Sn_2PO_4I: An Excellent Birefringent Material with Giant Optical Anisotropy in Non π-Conjugated Phosphate, *Angew. Chem., Int. Ed.*, 2021, **60**, 24901–24904.
16 G. Zou, C. Lin, H. Jo, G. Nam, T.-S. You and K. M. Ok, Pb_2BO_3Cl: A Tailor–Made Polar Lead Borate Chloride with Very Strong Second Harmonic Generation, *Angew. Chem., Int. Ed.*, 2016, **55**, 12078–12082.
17 Q. Wei, C. He, K. Wang, X. F. Duan, X. T. An, J. H. Li and G. M. Wang, $Sb_6O_7(SO_4)_2$: A Promising Ultraviolet Nonlinear Optical Material with an Enhanced Second-Harmonic-Generation Response Activated by Sb^{III} Lone-Pair Stereoactivity, *Chem. – Eur. J.*, 2021, **27**, 5880–5884.
18 H. W. Huang, L. J. Liu, S. F. Jin, W. J. Yao, Y. H. Zhang and C. T. Chen, Deep-Ultraviolet Nonlinear Optical Materials: $Na_2Be_4B_4O_{11}$ and $LiNa_5Be_{12}B_{12}O_{33}$, *J. Am. Chem. Soc.*, 2013, **135**, 18319–18322.
19 M. Mutailipu, M. Zhang, H. P. Wu, Z. H. Yang, Y. H. Shen, J. L. Sun and S. L. Pan, $Ba_3Mg_3(BO_3)_3F_3$ polymorphs with reversible phase transition and high performances as ultraviolet nonlinear optical materials, *Nat. Commun.*, 2018, **9**, 3089.
20 C. Wu, L. Lin, T. Wu, Z. Huang and C. Zhang, Deep-ultraviolet transparent alkali metal–rare earth metal sulfate $NaY(SO_4)_2{\cdot}H_2O$ as a nonlinear optical crystal: Synthesis and characterization, *CrystEngComm*, 2021, **23**, 2945–2951.
21 S. G. Zhao, X. Y. Yang, Y. Yang, X. J. Kuang, F. Q. Lu, P. Shan, Z. H. Sun, Z. S. Lin, M. C. Hong and J. H. Luo, Non-Centrosymmetric $RbNaMgP_2O_7$ with Unprecedented Thermo-Induced Enhancement of Second Harmonic Generation, *J. Am. Chem. Soc.*, 2018, **140**, 1592–1595.
22 H. W. Yu, J. S. Young, H. P. Wu, W. G. Zhang, J. M. Rondinelli and P. S. Halasyamani, $M_4Mg_4(P_2O_7)_3$ (M = K, Rb): Structural Engineering of Pyrophosphates for Nonlinear Optical Applications, *Chem. Mater.*, 2017, **29**, 1845–1855.
23 P. Yu, L. M. Wu, L. J. Zhao and L. Chen, Deep-Ultraviolet Nonlinear Optical Crystals: $Ba_3P_3O_{10}X$ (X = Cl, Br), *J. Am. Chem. Soc.*, 2014, **136**, 480–487.
24 S. G. Zhao, P. F. Gong, S. Y. Luo, L. Bai, Z. S. Lin, Y. Y. Tang, Y. L. Zhou, M. C. Hong and J. H. Luo, Tailored Synthesis of a Nonlinear Optical Phosphate with a Short Absorption Edge, *Angew. Chem.*, 2015, **127**, 4291–4295.
25 S. G. Zhao, P. F. Gong, S. Y. Luo, L. Bai, Z. S. Lin, C. M. Ji, T. L. Chen, M. C. Hong and J. H. Luo, Deep-Ultraviolet Transparent Phosphates $RbBa_2(PO_3)_5$ and $Rb_2Ba_3(P_2O_7)_2$ Show Nonlinear Optical Activity from Condensation of $[PO_4]^{3-}$ Units, *J. Am. Chem. Soc.*, 2014, **136**, 8560–8563.
26 M. Abudoureheman, S. J. Han, B. H. Lei, Z. H. Yang, X. F. Long and S. L. Pan, $KPb_2(PO_3)_5$: a novel nonlinear optical lead polyphosphate with a short deep-UV cutoff edge, *J. Mater. Chem. C*, 2016, **4**, 10630–10637.
27 B. B. Zhang, G. P. Han, Y. Wang, X. L. Chen, Z. H. Yang and S. L. Pan, Expanding Frontiers of Ultraviolet Nonlinear Optical Materials with Fluorophosphates, *Chem. Mater.*, 2018, **30**, 5397–5403.
28 L. Xiong, J. Chen, J. Lu, C. Y. Pan and L. M. Wu, Monofluorophosphates: A new source of deep-ultraviolet nonlinear optical materials, *Chem. Mater.*, 2018, **30**, 7823–7830.
29 J. Lu, J. N. Yue, L. Xiong, W. K. Zhang, L. Chen and L. M. Wu, Uniform alignment of non-π-conjugated species enhances deep ultraviolet optical nonlinearity, *J. Am. Chem. Soc.*, 2019, **141**, 8093–8097.
30 Z. Y. Bai and K. M. Ok, Designing Sulfate Crystals with Strong Optical Anisotropy through π-Conjugated Tailoring, *Angew. Chem., Int. Ed.*, 2023, e202315311.
31 X. F. Wang, X. D. Leng, Y. Kuk, J. Lee, Q. Jing and K. M. Ok, Deep-Ultraviolet Transparent Mixed Metal Sulfamates with Enhanced Nonlinear Optical Properties and Birefringence, *Angew. Chem., Int. Ed.*, 2023, e202315434.
32 X. Hao, M. Luo, C. S. Lin, G. Peng, F. Xu and N. Ye, M $(NH_2SO_3)_2$ (M=Sr, Ba): Two Deep-Ultraviolet Transparent Sulfamates Exhibiting Strong Second Harmonic Generation Responses and Moderate Birefringence, *Angew. Chem., Int. Ed.*, 2021, **60**, 7621–7625.
33 H. T. Tian, N. Ye and M. Luo, Sulfamide: A Promising Deep-Ultraviolet Nonlinear Optical Crystal Assembled from Polar Covalent $[SO_2(NH_2)_2]$ Tetrahedra, *Angew. Chem., Int. Ed.*, 2022, **61**, e202200395.
34 H. T. Tian, C. S. Lin, X. Zhao, S. H. Fang, H. Li, C. Wang, N. Ye and M. Luo, Design of a new ultraviolet nonlinear optical material $KNO_3SO_3NH_3$ exhibiting an unexpected strong second harmonic generation response, *Mater. Today Phys.*, 2022, **28**, 100849.
35 E. Hobbs, D. E. C. Corbridge and B. Raistrick, The crystal structure of monosodium phosphoramidate, $NaHPO_3NH_2$, *Acta Crystallogr.*, 1953, **6**, 621–626.
36 G. M. Sheldrick, A short history of SHELX, *Acta Crystallogr.*, 2008, **A64**, 112–122.
37 G. M. Sheldrick and T. R. Schneider, SHELXL: High-resolution refinement, *Methods Enzymol.*, 1997, **277**, 319–343.
38 A. M. Rappe, K. M. Rabe, E. Kaxiras and J. D. Joannopoulos, Erratum: Optimized pseudopotentials, *Phys. Rev. B: Condens. Matter Mater. Phys.*, 1990, **41**, 1227–1230.
39 J. P. Perdew, K. Burke and M. Ernzerhof, Generalized Gradient Approximation Made Simple, *Phys. Rev. Lett.*, 1997, **78**, 1396–1396.
40 D. J. Moss, E. Ghahramani, J. E. Sipe and H. M. van Driel, Band-structure calculation of dispersion and anisotropy in $\chi{\rightarrow}^{(3)}$ for third-harmonic generation in Si, Ge, and GaAs,

Phys. Rev. B: Condens. Matter Mater. Phys., 1990, **41**, 1542–1560.

41 W. D. Cheng, C. S. Lin, H. Zhang and G. L. Chai, Theoretical Evaluation on Terahertz Source Generators from Ternary Metal Chalcogenides of PbM_6Te_{10} (M = Ga, In), *J. Phys. Chem. C*, 2018, **122**, 4557–4564.

42 M. H. Lee, C. H. Yang and J. H. Jan, Band-resolved analysis of nonlinear optical properties of crystalline and molecular materials, *Phys. Rev. B: Condens. Matter Mater. Phys.*, 2004, **70**, 235110.

43 X. X. Jiang, S. G. Zhao, Z. S. Lin, J. H. Luo, P. D. Bristowe, X. G. Guan and C. C. Tian, The role of dipole moment in determining the nonlinear optical behavior of materials: ab initio studies on quaternary molybdenum tellurite crystals, *J. Mater. Chem. C*, 2014, **2**, 530.

44 D. H. Lin, M. Luo, C. S. Lin, F. Xu and N. Ye, KLi$(HC_3N_3O_3)\cdot 2H_2O$: Solvent-drop Grinding Method toward the Hydro-isocyanurate Nonlinear Optical Crystal, *J. Am. Chem. Soc.*, 2019, **141**, 3390–3394.

45 S. K. Kurtz and T. T. Perry, A powder technique for the evaluation of nonlinear optical materials, *J. Appl. Phys.*, 1968, **39**, 3798–3813.

46 W. Cheng, C. Lin, H. Lin and G. Chai, Theoretical Evaluation on Terahertz Source Generators from Ternary Metal Chalcogenides of PbM_6Te_{10} (M = Ga, In), *J. Phys. Chem. C*, 2018, **122**, 4557–4564.

47 C. T. Chen, Y. C. Wu and R. K. Li, The anionic group theory of the non-linear optical effect and its applications in the development of new high-quality NLO crystals in the borate series, *Int. Rev. Phys. Chem.*, 1989, **8**, 65–91.

48 L. Cao, G. Peng, W. Liao, T. Yan, X. Long and N. Ye, A microcrystal method for the measurement of birefringence, *CrystEngComm*, 2020, **22**, 1956–1961.

49 H. T. Tan, C. S. Lin, Y. Q. Zhou, X. Zhao, H. X. Fan, T. Yan, N. Ye and M. Luo, Design of the Ionic Organic Nonlinear Optical Material $NH_4[LiC_3H(CH_3)O_4]$ with Ultrawide Band Gap and Moderate Birefringence, *Angew. Chem., Int. Ed.*, 2023, **62**, e202304858.

